PHYSICAL CONDITIONS IN THE LOW-IONIZATION BROAD-LINE REGION IN ACTIVE GALAXIES

S. PANDA[1,2]

[1] *Center for Theoretical Physics, Polish Academy of Sciences, Al. Lotników 32/46, 02-668 Warsaw, Poland*
E–mail panda@cft.edu.pl.

[2] *Nicolaus Copernicus Astronomical Center, Polish Academy of Sciences, ul. Bartycka 18, 00-716 Warsaw, Poland*

Abstract. Resolving the complexity in FeII species in quasar spectra has been an ongoing work for over 40 years. First identified and reported for the prototypical Narrow-line Seyfert 1 galaxy, I Zw 1 (Phillips 1978), the study has made a niche of its own in the field of AGN research. Seminal works led by Boroson & Green (1992), Verner et al. (1999), Sigut & Pradhan (2003) and others encapsulate the 'yet to be complete' understanding of the physics of the line formation for this first-ionized state of iron (FeII). A major part of the puzzle is lent by the sheer number of spectral lines in FeII that spans across a wide energy range (from UV to NIR). This extended emission seen in the spectra mimics a continuum of sorts, thus the telltale term *pseudo-continuum*. Gaining knowledge from the past studies and of our own, in this study we search for a reliable proxy to FeII. This proxy, CaII, is a much simpler ionic species which is characterized by its triplet in the near-infrared part of an AGN spectrum. The analogous line excitation mechanisms (dominated by the Lyα fluorescence and collisional excitation) for the production of these two species is confirmed by the tight correlation between the respective line strengths that we observe from our up-to-date collection of coincident measurements in the optical and NIR, and re-affirmed by our photoionization models. Additionally, our models constrain the physical parameters, such as the required level of ionization and the density of the medium, i.e. the broad-line region (BLR), that contain these ionic species, hinting also to the cloud's composition and structure (Panda et al. 2020; Panda 2020). This study reveals the utility of the CaII as a proxy for FeII in ways more than one, primarily, establishing a new radius-luminosity relation and in quasar main sequence studies.

1. INTRODUCTION

The complexity of FeII is majorly due to the numerous transition lines this first ionized state of Fe has, spreading across the near infrared (NIR) to ultraviolet (UV) wavelengths (Boroson & Green 1992, Bruhweiler & Verner 2008, Garcia-Rissmann et al. 2012) which makes it quite complicated to be modelled. The difficulty in understanding the FeII emission has led us in search of other reliable, simpler ionic species such as CaII and O I (Martínez-Aldama et al. 2015 and references therein) which would originate from the same part of the BLR and could play a similar role in quasar main sequence studies. Here, the CaII emission refers to the *Ca triplet* (CaT), i.e., the IR triplet emitting at λ8498Å, λ8542Å and λ8662Å. We refer the readers to Panda et al. (2020) for an overview on the issue of CaT emission in AGNs and its relevance to the FeII emission.

2. METHOD & ANALYSIS

We make use of a subset of the photoionization models executed in Panda (2020) using CLOUDY (v17.02, Ferland et al. 2017) which covers a wide range of parameter space, i.e. varying the cloud particle density, $10^{10.5} \leq \mathrm{n_H} \leq 10^{13}$ (cm^{-3}), the ionization parameter, $-4.25 \leq \log \mathrm{U} \leq -1.5$, the metallicity, $0.1\mathrm{Z}_{\odot} \leq \mathrm{Z} \leq 10\mathrm{Z}_{\odot}$, at a base cloud column density, 10^{24} cm^{-2}. We utilize the spectral energy distribution (SED) for the nearby (z= 0.061) NLS1, I Zw 1[1]. In this paper, we concentrate only on the metallicity case at solar ($\mathrm{Z}_{\odot}$) and at $10\mathrm{Z}_{\odot}$. Furthermore, an additional set of models were performed that included a non-zero microturbulence value, i.e. at 20 $\mathrm{km\,s^{-1}}$. This value of microturbulence has been shown in our previous works (Panda et al. 2018, 2019, Panda 2020) to aid in further increase in the optical FeII emission. We focus on the four low-ionization lines (LILs, IP < 20 eV) that are confined in the broad-line clouds, i.e. Hβ, the optical FeII blend[2], O I λ8446[3] and CaT; and extract the information about their line emission by estimating their line equivalent widths (EWs). The EWs are estimated using continua appropriate for the emission lines in consideration obtained from the models, e.g. a continuum luminosity at 4885.36Å for the Hβ and the optical FeII blend, and one at 8329.26Å for the O I λ8446 and CaT.

A vital information to constrain the emitting region of these lines is given by their distance from the ionizing source, the radius of the BLR (R_{BLR}) in this case. The R_{BLR} can be inferred using the photoionization theory,

$$R_{BLR}\ [cm] = \sqrt{\frac{Q(H)}{4\pi U n_H c}} \equiv \sqrt{\frac{L_{bol}}{4\pi h\nu\ U n_H c}} \simeq \frac{2.294\times 10^{22}}{\sqrt{U n_H}} \quad (1)$$

where, R_{BLR} is the distance of the emitting cloud from the ionizing source which has a mean local density $\mathrm{n_H}$ and receives an ionizing flux that is quantified by the ionization parameter, U. $Q(H)$ is the number of ionizing photons, which can be equivalently expressed in terms of the bolometric luminosity of the source per unit energy of a single photon, i.e. hν. Here, we consider the average photon energy, hν = 1 Rydberg (Wandel et al. 1999, Marziani et al. 2015). The bolometric luminosity of I Zw 1 is $\mathrm{L_{bol}} \sim 4.32 \times 10^{45}$ erg s^{-1}. This is obtained by applying the bolometric correction prescription from Netzer (2019) on I Zw 1's $\mathrm{L_{5100}} \sim 3.48 \times 10^{44}$ erg s^{-1} (Persson 1988).

3. RESULTS & DISCUSSIONS

CLOUDY calculates the equivalent width by assuming a 100% covering factor[4]. Baldwin et al. (2004) showed that a covering factor of ≈ 20% is a good indicator of a successful

[1]The I Zw 1 ionizing continuum shape is obtained from NASA/IPAC Extragalactic Database.

[2]the optical FeII emission blue-ward of the Hβ emission line within λ4434-4684 Å.

[3]the NIR emitting lines at λ8446.25Å, λ8446.36Å and λ8446.76Å.

[4]Covering factor or CF is defined as the fraction of 4π sr covered by the clouds, as seen from the central black hole. Normally, the CF is expressed as $\Omega/4\pi$, where Ω is the solid angle.

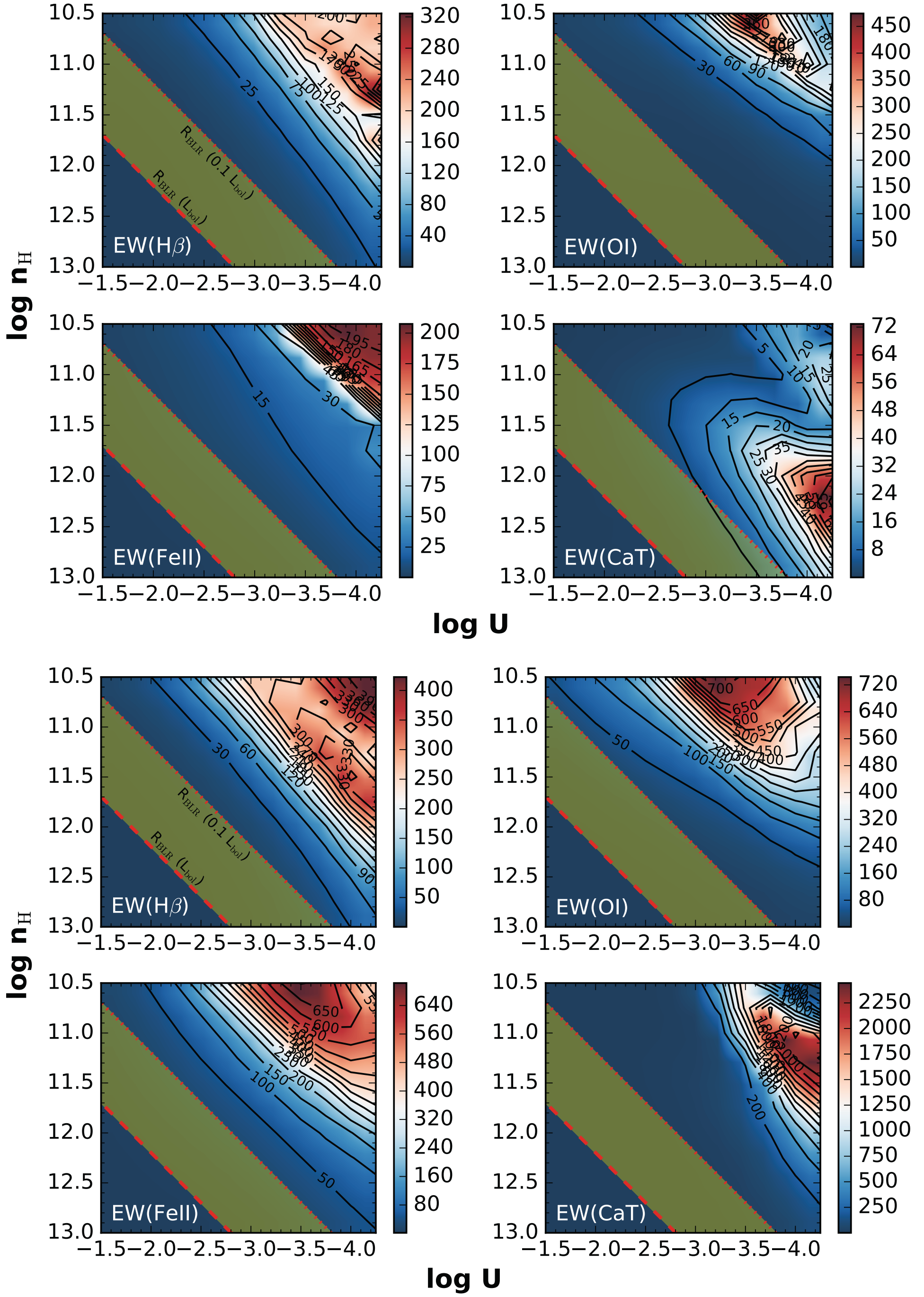

Figure 1: Base model at Z = $Z_\odot$ (*UPPER*) vs at Z = $10Z_\odot$ (*LOWER*) at zero microturbulence. The colorbar and the contours mark the EWs of the respective lines considering a 20% CF. The shaded region depicts the inferred size of the BLR using Equation 1 for $10\%L_{\rm bol}$ and at $L_{\rm bol}$ for `I Zw 1`.

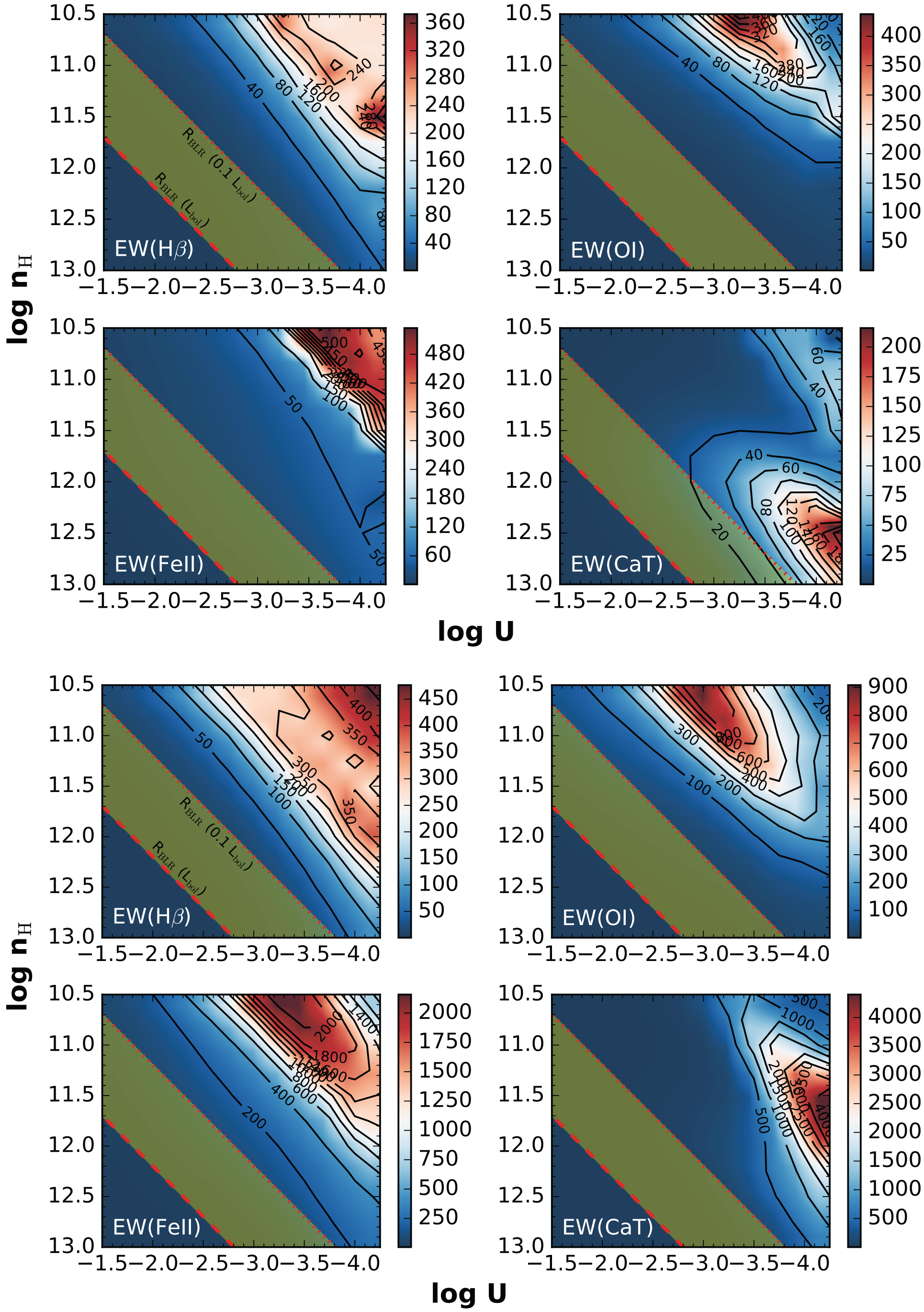

Figure 2: Base model at $Z = Z_\odot$ (*UPPER*) vs at $Z = 10Z_\odot$ (*LOWER*) at $20\,\mathrm{km\,s^{-1}}$. The colorbar and the contours mark the EWs of the respective lines considering a 20% CF. The shaded region depicts the inferred size of the BLR using Equation 1 for $10\%L_{\mathrm{bol}}$ and at L_{bol} for `I Zw 1`.

model. A typical `CLOUDY` predicted equivalent width of > 400 Å is consistent with the observed value with a ∼20% of covering factor. We utilize this value of CF to estimate the EWs for the four LILs in our analysis.

3. 1. NEED FOR HIGHER-THAN-SOLAR METALLICITY IN THE BLR

In Figure 1, we illustrate the distribution of the EWs for the four LILs in the $\log \mathrm{U} - \log \mathrm{n_H}$ diagram. The two sets of illustration correspond to two selected cases of metal content in the BLR cloud - at solar metallicity ($\mathrm{Z_\odot}$) and at $10\mathrm{Z_\odot}$. In our earlier studies (Panda et al. 2018, 2019, 2020, Panda 2020), we have found in order to reproduce the required FeII emission for sources with significantly high FeII strength ($\mathrm{R_{FeII}}$[5] $\gtrsim 1$), higher metal content is required in addition to relatively high number density (i.e. $\sim 10^{12}$ cm^{-3}) and cloud sizes that are of the same order (this requires to set a cloud column density $\sim 10^{24}$ cm^{-2}). The shape of the ionizing continuum has also a role to play to provide sufficient number of ionizing photons carrying energies up to 1 Rydberg (Panda et al. 2020). The panels for the solar metallicity case in Figure 1 show a preference of a low-ionization ($-4.25 \leq \log \mathrm{U} \leq -3.0$), relatively low density ($10^{10.5} \leq \mathrm{n_H} \leq 10^{11.5}$ cm^{-3}) for the Hβ and FeII, while this is slightly shifted to higher ionization values and lower densities for O I λ8446. For CaT, the emission is quite spread out in terms of the EWs recovered, with densities covering the full range assumed in the models, albeit the fact that the ionization levels are similar to the other lines. We have found in Panda (2020) that an optimum metallicity requirement for the FeII and CaT emission for `I Zw 1` is $\gtrsim 10\mathrm{Z_\odot}$, with CaT emission able to be significant even at lower metal content (but above solar values). Another key to the issue is the location of the BLR cloud from the ionizing source, i.e. the accretion disk. This is illustrated in the panels wherein we use Eq. 1 and assume two cases for the bolometric luminosity - at 10% and 100%. The former case has been tested in our previous work (Panda 2020) that infers perfect agreement of the radial size from photoionization to the reverberation-mapped radius for this source. This implies that the continuum that the BLR *sees* is different from what a distant observer perceives. The inferred EWs within this highlighted zone in Figure 1 suggest EWs < 15Å(in solar case) for Hβ, O I λ8446 and FeII, and ∼ 5Å for CaT. This then implies a quite low value for $\mathrm{R_{FeII}}$ (∼0.6) and equivalently for $\mathrm{R_{CaT}}$ (i.e., ratio of the CaT emission to the Hβ, ∼0.4). This issue gets resolved in the $10\mathrm{Z_\odot}$ models where the EWs recovered are sufficient to provide strengths of FeII and CaT that are identical to the observed estimates (Persson 1988, Marinello et al. 2016). It is also worth noticing that the increase in the metal content pushes the CaT emission closer to the other three lines.

3. 2. PUSHING THE LIL EMISSION: CHAOTIC MOTIONS WITHIN THE BLR

Local turbulence substantially affects the FeII spectrum in photoionization models by facilitating continuum and line-line fluorescence. Increasing the turbulence can increase the FeII strength and give better agreement between the predicted shape of the FeII blends and observation (Shields et al. 2010). The effect of the microturbulence has been carefully investigated in our previous works (Panda et al. 2018, 2019, Panda 2020) where a systematic rise in the $\mathrm{R_{FeII}}$ estimates is obtained by increasing the microturbulence up to 10-20 km s^{-1}. We test this in the context of this work

[5] i.e., the ratio of the integrated FeII emission in the optical blue-wards of the broad Hβ line to the Hβ emission.

and the results are illustrated in Figure 2. The individual lines' EWs rises by up to $\sim$2 times when the turbulence in the medium is raised from 0 to 20 $\mathrm{km\,s^{-1}}$, and the inferred R_{FeII} values are higher for models with 20 $\mathrm{km\,s^{-1}}$ turbulence. The case with 20 $\mathrm{km\,s^{-1}}$ and $10Z_\odot$ results in bringing all the four species in agreement in terms of the parameter space occupied by them. Their individual behaviour needs further investigation and will be explored in a future work.

Acknowledgements

The project was partially supported by the Polish Funding Agency National Science Centre, project 2017/26/A/ST9/00756 (MAESTRO 9) and MNiSW grant DIR/WK/2018/12.

Softwares: `CLOUDY` v17.02 (Ferland et al. 2017); `MATPLOTLIB` (Hunter 2007); `NUMPY` (Oliphant 2015)

References

Baldwin, J. A., Ferland, G. J., Korista, K. T. et al.: 2004, *ApJ*, **615**, 610.
Boroson, T. A., Green, R. F.: 1992, *ApJS*, **80**, 109.
Bruhweiler, F., Verner, E.: 2008, *ApJ*, **675**, 83.
Ferland, G. J., Chatzikos, M., Guzmán, F. et al.: 2017, *RMxAA*, **53**, 385.
Garcia-Rissmann, A., Rodríguez-Ardila, A., Sigut, T. A. A., Pradhan, A. K.: 2012, *ApJ*, **751**, 7.
Hunter, J. D.: 2007, *Computing in Science and Engineering*, **9**, 90.
Marinello, M., Rodríguez-Ardila, A., Garcia-Rissmann, A. et al.: 2016, *ApJ*, **820**, 116.
Martínez-Aldama, M. L., Dultzin, D., Marziani, P. et al.: 2015, *ApJS*, **217**, 3.
Marziani, P., Sulentic, J. W., Negrete, C. A. et al.: 2015, *ApSS*, **356**, 339.
Netzer, H.: 2019, *MNRAS*, **488**, 5185.
Oliphant, T.: 2015, *NumPy: A guide to NumPy*, 2nd edn., CreateSpace Independent Publishing Platform, USA, http://www.numpy.org/http://www.numpy.org/
Panda, S., Czerny, B., Adhikari, T. P. et al.: 2018, *ApJ*, **866**, 115.
Panda, S., Czerny, B., Done, C., Kubota, A., 2019, *ApJ*, **875**, 133.
Panda, S., Martínez-Aldama, M. L., Marinello, M. et al.: 2020, *ApJ*, **902**, 76.
Panda, S.: 2020, arXiv e-prints, arXiv:2004.13113.
Persson, S. E.: 1988, *ApJ*, **330**, 751.
Phillips, M. M.: 1978, *ApJ*, **226**, 736.
Shields, G. A., Ludwig, R. R., Salviander, S.: 2010, *ApJ*, **721**, 1835.
Sigut, T. A. A., Pradhan, A. K.: 2003, *ApJS*, **145**, 15.
Verner, E. M., Verner, D. A., Korista, K. T. et al.: 1999, *ApJS*, **120**, 101.
Wandel, A., Peterson, B. M., Malkan, M. A.: 1999, *ApJ*, **526**, 579.